ECS The Electrochemical Society
Advancing solid state & electrochemical science & technology

Operando Ultrasonic Monitoring of Lithium-Ion Battery Temperature and Behaviour at Different Cycling Rates and under Drive Cycle Conditions

View the article online for updates and enhancements.

CrossMark

Operando Ultrasonic Monitoring of Lithium-Ion Battery Temperature and Behaviour at Different Cycling Rates and under Drive Cycle Conditions

Rhodri E. Owen,[1,2,z] James B. Robinson,[1,2] Julia S. Weaving,[1,2] Martin T. M. Pham,[1] Thomas G. Tranter,[1,2] Tobias P. Neville,[1] Duncan Billson,[3] Michele Braglia,[4] Richard Stocker,[4] Annika Ahlberg Tidblad,[5,6] Paul R. Shearing,[1,2] and Dan J. L. Brett[1,2,z]

[1]*Electrochemical Innovation Lab, Department of Chemical Engineering, University College London, London, WC1E 7JE, United Kingdom*
[2]*The Faraday Institution, Harwell Science and Innovation Campus, Didcot, OX11 0RA, United Kingdom*
[3]*School of Engineering, University of Warwick, Coventry, CV4 7AL, United Kingdom*
[4]*HORIBA MIRA Ltd., Nuneaton, Warwickshire, CV10 0TU, United Kingdom*
[5]*Volvo Car Corporation, SE-405 31, Gothenburg, Sweden*
[6]*The Angstrom Advanced Battery Centre, Department of Chemistry, Uppsala University, SE-751 21 Uppsala, Sweden*

Effective diagnostic techniques for Li-ion batteries are vital to ensure that they operate in the required voltage and temperature window to prevent premature degradation and failure. Ultrasonic analysis has been gaining significant attention as a low cost, fast, non-destructive, operando technique for assessing the state-of-charge and state-of-health of Li-ion batteries. Thus far, the majority of studies have focused on a single C-rate at relatively low charge and discharge currents, and as such the relationship between the changing acoustic signal and C-rate is not well understood. In this work, the effect of cell temperature on the acoustic signal is studied and shown to have a strong correlation with the signal's time-of-flight. This correlation allows for the cell temperature to be inferred using ultrasound and to compensate for these effects to accurately predict the state-of-charge regardless of the C-rate at which the cell is being cycled. Ultrasonic state-of-charge monitoring of a cell during a drive cycle illustrates the suitability of this technique to be applied in real-world situations, an important step in the implementation of this technique in battery management systems with the potential to improve pack safety, performance, and efficiency:

As a result of their high energy and power densities, long cycle life, and relatively low cost, lithium-ion batteries (LIBs) have received significant attention in the fields of electric vehicles (EVs) and consumer electronics.[1] A LIB must operate in a restricted voltage and temperature window to prevent premature capacity degradation, failure, and potentially severe safety issues.[2] As such, the implementation of a battery management system (BMS) is vital for the safe and reliable operation of any LIB module or pack, these systems ensure that the cells are operating within these safety limits as well as ensuring that the cells' state-of-charge (SoC) is balanced. To achieve this, they require information on the SoC, state-of-health (SoH), and temperature of the cells. More information about each individual cell allows for the BMS to operate more efficiently and safely.[2]

State estimation of LIBs in BMSs is usually achieved through the use of a combination of the open-circuit voltage (OCV) of the cell as well as "Coulomb counting" and capacity measurements.[3] While these techniques are widely employed, there are still issues associated with their accuracy.[4] Sufficient time must be provided for the OCV of a LIB to equilibrate to achieve an accurate measurement, readings conducted while batteries are operating can result in poor accuracy.[5] Coulomb counting techniques require information on the initial SoC and accurate current measurements, even small errors can become significant due to the cumulative nature of the technique.[4] Any additional information or improved accuracy of state estimation and temperature will result in a more effective BMS with potential benefits to cell performance and life.

One state estimation technique that is attracting increasing attention at present is the use of acoustics. The technique involves the analysis of cells using ultrasonic waves and represents a non-destructive, cost-effective, and rapid method that can be used *operando*.[6,7] Sood et al. published one of the first studies using this technique and demonstrated that by studying the time-of-flight (ToF) and amplitude of ultrasound waves through a LIB, the difference between a fresh cell and one that had failed catastrophically could be easily determined.[8] An extensive study by Hsieh and coworkers showed how the technique could be utilized to monitor the SoC of numerous cell geometries and chemistries.[9] Long-term cycling has shown that the technique can also be used to monitor the degradation of the cell with cycle number and measure the SoH.[10] Similar work by Ladpli and coworkers has shown that an ultrasound-guided wave method can be used similarly to determine SoC and SoH.[11–13] While the vast majority of studies have focused on single-point measurements, other studies have shown the technique can also be used to map the surface of a cell and monitor the extent of these changes at various points within the cell as well as to detect the position of any defects that may be present.[14,15]

The majority of studies reported thus far have cycled cells at relatively low (e.g. C/20) and constant C-rates that are not applicable to most real-world applications, particularly the high charge and discharge rates required for EV applications. In most applications, it is also unlikely that a cell would be discharged at a constant rate and as such the technique must be able to still predict SoC and SoH under rapidly altering currents. A recent study has shown that the rate at which a cell is charged or discharged can have a significant effect on the changes in the acoustic signal.[16] Popp and co-workers, using a similar guided wave technique, also observed that the ToF variation with SoC was dependent on the charge and discharge rate.[17] Similar results showing the dependence of acoustic change on C-rate have also been reported by Chang et al.[18] If an ultrasonic technique is to be applied, *operando*, to monitor cells in operation and inform BMSs, a good understanding of how and why C-rate influences the acoustic signal and the technique's ability to monitor SoC and SoH is required.

zE-mail: Rhodri.owen@ucl.ac.uk; D.Brett@ucl.ac.uk

Experimental

Ultrasonic measurements were conducted in pulse-echo mode using an EPOCH 650 ultrasound non-destructive flaw detector (Olympus Crop., Japan) and a 6 mm diameter, 5 MHz, M110-RM transducer (Olympus Corp., Japan). The EPOCH 650 was controlled using custom Python code which allowed for data collection at desired intervals up to $0.5\,s^{-1}$. All experiments were performed using commercial 210 mAh pouch cells (PL-65168–2C, AA Portable Power Corp., U.S.A) composed of a $LiCoO_2$ (LCO) cathode and a graphite anode. These cells have been studied previously [19–21] and were chosen to minimize temperature gradients both across the surface of the cell and through the thickness. The size of the transducer relative to the surface of the pouch ensures that the ultrasonic signal is representative of the changes occurring to the whole cell. Contact between the transducer and cell was maintained using a small quantity of H-2 high-temperature ultrasonic couplant (Olympus Corp., Japan). To ensure repeatable readings a custom-designed, 3D printed holder was used with a 250 g weight applied to ensure a constant and repeatable pressure on the transducer. Acoustic waveforms were collected at 30 s intervals alternating between a low gain setting for the analysis of all peaks and a high gain setting for the analysis of the peaks at a higher time-of-flight. Peak amplitude is reported as a percentage of highest positive and lowest negative, saturated peaks. Analysis of the acoustic data was conducted using Python 3.7. For clarity, all of the acoustic signals were + half-wave rectified before the plotting of the colourmaps, eliminating any negative peaks.

Cell cycling was conducted using a Gamry Interface 1010E potentiostat (Gamry Instruments, U.S.A.). All cells were used as received and were cycled in accordance with the manufacturer's specifications. They were charged at a constant current (1 C, C/2, or C/5) to 4.2 V where the cell was then held at this voltage until the current fell to 10.5 mA. The discharge step of the cycling was conducted at a constant current (1 C, C/2, or C/5) until the voltage dropped to 2.75 V. Acoustic readings were conducted concurrently. The drive cycle test was designed based on data reported by Kellner et al.[22,23] with acoustic waveforms collected at 2 s intervals. SoC is reported as a percentage of the measured capacity of each cell after the first cycle, depth-of-discharge (DoD) is reported as a percentage of the measured capacity that has been removed from a fully charged cell.

The temperature of the cell was monitored using a K-Type thermocouple on the surface of the cell. Temperature logging was achieved using a TC-08 thermocouple interface (PicoTech, U.K.) and PicoLog software (PicoTech, U.K.). Cells were cycled at room temperature, any experiments requiring the cell to be heated or cooled were conducted in a Maccor MTC-020 temperature chamber with a K-type thermocouple placed on the cell's surface to monitor the temperature.

X-ray computed tomography (CT) images of the pouch cells studied were collected using a Nikon XT-225 (Nikon Metrology, U.K.). A tungsten target with a 1 mm copper filter, an accelerating voltage of 130 kV, and an incident beam power of 13 W was used for the scans. The radiographic images were reconstructed using "Nikon CT Agent," visualization of the reconstructed datasets was performed using Aviso Fire 9.4 (Thermo Fisher Scientific, U.S.A.).

Results

The ultrasonic signal generated by a pouch cell.—Ultrasonic testing is a non-destructive diagnostic technique that relies on monitoring how ultrasound waves propagate and pass through a sample of interest. While the technique is used extensively for testing metals and welds for cracks and defects, its use for analyzing and monitoring batteries is relatively new.[5,7] Typically, a short longitudinal ultrasonic pulse is generated by a piezoelectric transducer, the wave then propagates through the material under investigation. The speed at which the wave travels, *c*, is dependent on the bulk (*K*) and shear (*G*) moduli of the material as well as the density, Eq. 1.

$$c = \sqrt{\frac{K + \frac{4}{3}G}{\rho}} \qquad [1]$$

The bulk and shear moduli of the material are related to the Young's modulus (*E*) and the Poisson's ratio (v) of the material by $K = E3(1 - 2v)$ Eq. 2 and $G = E2(1 + v)$ Eq. 3.

$$K = \frac{E}{3(1 - 2v)} \qquad [2]$$

$$G = \frac{E}{2(1 + v)} \qquad [3]$$

As the signal travels through the material under study the amplitude will gradually decrease as energy is lost. The processes related to the wave's attenuation are complex, with the loss in energy related to both absorption and scattering effects. The acoustic attenuation (*Z*) is related to the density and Young's modulus of the material the wave is travelling through, $Z = \rho E$ Eq. 4.

$$Z = \sqrt{\rho E} \qquad [4]$$

When the acoustic signal hits the interface between two materials with different acoustic impedances (*Z*) some of the signal is reflected
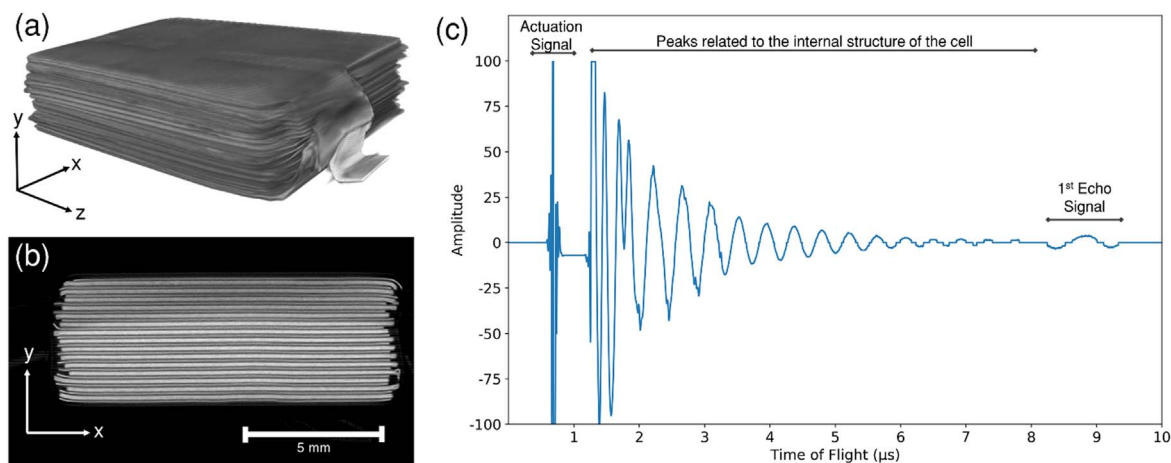

Figure 1. (a) 3D volume rendering of the internal electrode stack structure of the 210 mAh cell under study. (b) an orthogonal slice of the electrode stack showing the alternating layered electrodes. (c) a typical acoustic signal obtained by probing a 210 mAh pouch cell using an ultrasonic pulse-echo technique.

while some is transmitted. The ratio of the transmitted signal to the reflected (R) is dependent on the magnitude of the difference between the acoustic impedance of the two materials and can be determined by $R = Z_2 - Z_1 Z_2 + Z_1$ Eq. 5

$$R = \frac{Z_2 - Z_1}{Z_2 + Z_1} \qquad [5]$$

A three-dimensional (3D) volume rendering of the internal electrode stack contained within one of the pouch cells was obtained by X-ray CT and is shown in Fig. 1a. An orthogonal slice of this structure is shown in Fig. 1b and shows the layered internal structure of the cell consisting of alternating layers of electrodes and separators. Each of these interfaces represents a point where the ultrasonic signal will be influenced with some of the signal reflected and some transmitted. A typical waveform obtained from pulse-echo probing of a 210 mAh pouch cell using ultrasound is shown in Fig. 1c. Below 1 μs a set of peaks related to the actuation of the transducer is observed. This remains unchanged regardless of any changes within the cell since it is generated by the pulse receiver. Between 1 and 8 μs, s decreasing with higher ToF values. These peaks are related to the internal structure of the cell and are likely generated at the interfaces between different materials present in the cell where there is a sufficient difference in acoustic impedances to cause some of the wave to be reflected rather than transmitted. As the wave passes deeper into the cell the amplitude of the wave decreases in part because progressively more has been reflected and also due to attenuation such as that described in $Z = \rho E$ Eq. 4. A signal of higher amplitude is observed at *ca.* 9 μs. This signal, sometimes referred to as the "first echo peak," is caused by the component of the ultrasound signal that has passed through the entire pouch cell and has reached the back.[24] At this point, due to the large difference in acoustic impedance of the air and the pouch cell packaging, the vast majority of the signal is reflected and not transmitted, resulting in a higher amplitude than the peaks in the 7–8 μs section since very little of the signal is transmitted.

Monitoring cell temperature using ultrasound.—It is crucial for the effect of temperature to be understood if ultrasound is to be used to monitor the cells while in operation. Not only will this allow for the decoupling of temperature effects at higher C-rates but will also allow the temperature of the whole cell to be monitored (inferred). To determine the effect of temperature, a cell left at an as-received open-circuit potential (3.7 V, *ca.* 30% SoC), was placed in a temperature chamber and held at a constant temperature of 25 °C for 1 h. After this period of time, the cell chamber was heated to 60 °C and held for a further 2 h, the chamber was then cooled to −10 °C and held for 2 h before finally being heated to room temperature. Figure 2a shows how the acoustic signal changed over the course of the experiment with the variation in cell temperature shown in Fig. 2b.

The effect of temperature on peaks at low times of flight is relatively small, this is consistent with the work conducted by Robinson et al. where the study focused only on a ToF range of 0–5 μs and an observed temperature shift of *ca.* 5 °C (relative to the *ca.* 75 °C range used in this study) and observed no significant changes.[16] The effect of temperature on the peak position increases as the initial ToF of the peaks increases. These results are expected since peaks present at higher initial ToF values result from reflections from deeper within the cell and as such pass through more of the cell. The "first echo" peak initially present at *ca.* 8.5 μs shows the largest deviation since the peak represents the signal that has travelled through the entire thickness of the cell and been reflected back. Not only does this peak show the largest change but it also gives information about the temperature of all layers within the cell. Peaks at earlier ToFs are related to reflections from within the cell and will only show changes occurring in the layers before the reflection occurs. The "first echo" peak should show changes

regardless of where the temperature change is occurring since the signal must travel through all layers twice before the reflected can be received. If, as expected, the signal is impacted by all electrodes within the cell, this opens up the possibility of detecting internal temperature changes and monitoring any cell damage occurring internally to potentially aid the detection and prevention of thermal runaway. Further experiments with internal temperature measurements would be required to confirm this is possible.

An increase in ToF may be related to a number of factors, as outlined earlier. As the cell is heated, the density of the materials within the cell are reduced which in turn affects the speed of sound through the material and as such the ToF. A similar reduction in speed and a concurrent increase in ToF due to decreases in density and changes in the elastic properties has been observed upon heating in various materials previously.[25,26] A change in electrolyte viscosity, which acts as a couplant through the whole cell, will also play a role.[27] Another factor potentially causing the increased ToF is the expansion of the cell as the electrode layers heat, a greater distance for the ultrasonic wave to travel due to this increased thickness would increase the ToF. Conversely, the increased density, higher electrolyte viscosity, and reduced cell thickness as the cell is cooled would also be in agreement with the observed decrease in ToF.[25–27]

As the cell is heated, the amplitude of the "first echo" peak is reduced and when the temperature decreases the "first echo" peak amplitude increases, this is shown in Fig. 2c where the 7.5–10 μs of the high gain test is shown. This increase in amplitude at lower temperatures may be related to factors such as cell contraction. In addition, the viscosity and density of the materials within the cell, particularly the electrolyte which penetrates all layers of the cell and allows for good acoustic transmission, will be affected, influencing the acoustic signal. Higher viscosity and a change in the elastic properties of the materials, as well as a shorter distance to travel through the cell due to the contraction, would all result in lower signal attenuation.

The ToF and amplitude of the "first echo" peak as a function of temperature is shown in Figs. 2d and 2e, respectively. A linear relationship between the ToF and temperature is observed, with a relationship such as this, for a given state-of-charge, the temperature of a cell may be monitored using pulse-echo acoustic ToF measurements. Monitoring the cell temperature using acoustics has several benefits over traditional methods with the main advantage being that any temperature changes occurring within the internal structure of the cell can also be detected rapidly since the signal passes through the whole cell, something not possible with surface-sensitive methods such as a thermocouple placed on the cell surface. It has been widely shown that internal thermal gradients are present in cells and in some failure cases these may be extremely large.[28–30] As discussed, the amplitude is also dependent on the cell temperature; however, this relationship is not linear, as shown in Fig. 2e.

Full analysis of the data shows that the ramp rate used for heating and cooling is sufficiently slow that the full cell has enough time to heat or cool with only minimal changes in acoustic signal observed in the hold period, which corresponds to the slow heating or cooling of the cell at these final temperatures. The linear relationship between temperature and ToF is maintained across this period.

If the cell temperature is monitored using both a surface thermocouple and the ultrasonic technique detailed here, there is the possibility that any deviation away from the linear relationship can be used to detect internal damage or internal heating (temperature gradients) of the cell, potentially providing a method to detect if the cell is approaching a thermal runaway event.

While the study summarized in Fig. 2 shows there is a linear relationship between temperature and ToF, these experiments were conducted on a cell at a single SoC (30%). As the cell charges and discharges, the material properties of both the anode and cathode will change, these changes will also be accompanied by a change in the thickness of the cathode and anode and as a result the thickness of the whole cell.[31] To understand how the SoC of the cell affects the
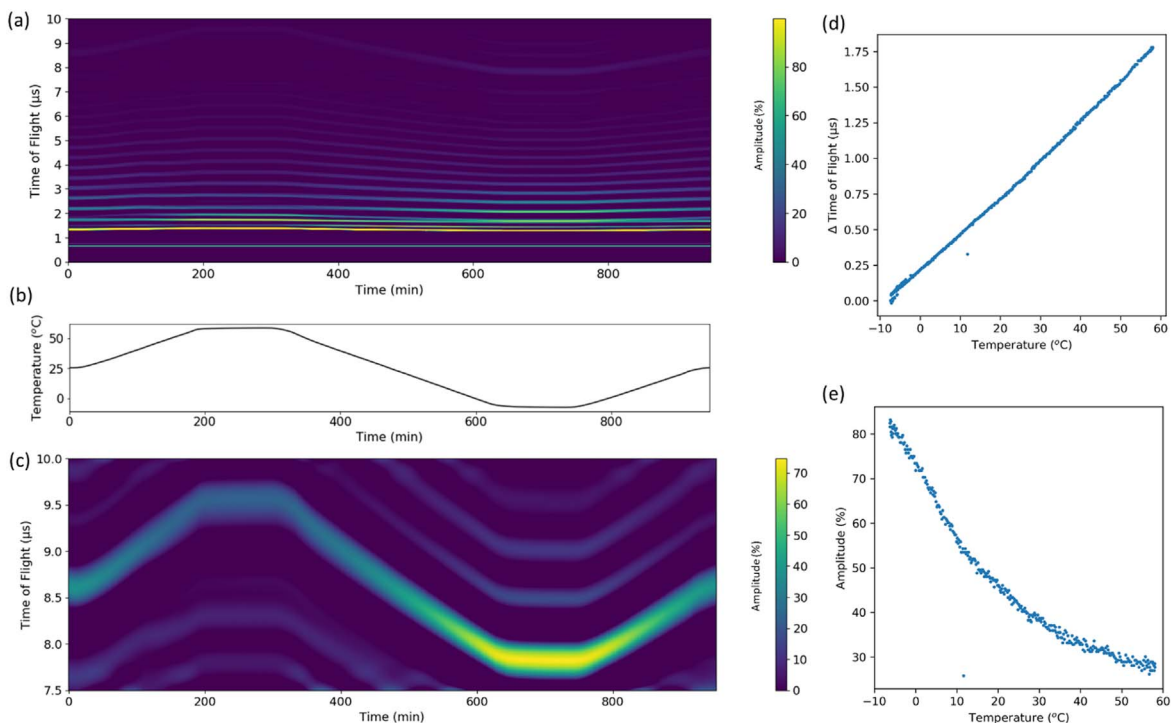
Figure 2. (a) A colourmap plot showing the change in the acoustic waveform as a 210 mAh pouch cell is heated and cooled (b) the temperature of the cell as it is heated and cooled. (c) A magnified colourmap plot of how the first echo peak varies as the cell is heated and cooled. (d) The linear relationship observed between the ToF of the first echo peak and temperature. (e) The relationship between the amplitude of the first echo peak and temperature.

relationship between the temperature and ToF of the "first echo" peak the experiment was repeated at six different SoCs. An overview of the results obtained from these tests is shown in Fig. 3.

The linear relationship between the time-of-flight of the "first echo" peak and the temperature is observed at all SoC in this temperature range (Fig. 3). There is, however, a slight difference in gradient as the SoC of the cell is increased. Some changes are to be expected since the properties of the materials are changing as the graphite and LCO are lithiated or delithiated which will, in turn, affect the coefficient of thermal expansion. A similar effect was reported by Oh et al. where they noted that for an NMC graphite cell the thermal expansion of a cell was dependent on the state-of-charge.[32] As the SoC decreases, the gradient of the line increases, meaning that at lower SoC the temperature has a more significant impact on the acoustic ToF. In their study, Oh et al. observed a similar phenomenon where at lower SoCs a larger expansion was observed for the same temperature change.[32] However, it must be stressed that factors other than cell thickness are likely to also play a significant role.

The subplot of Fig. 3 shows how the calculated gradient changes with each SoC. Again, a linear relationship is observed, indicating that it should be possible to predict the gradient and how it changes based on the SoC. Using the information obtained from these experiments, it should be possible to measure the cell temperature based purely on acoustic measurements as long as the SoC of the cell is known.

Effect of SoC on acoustic signal.—To gain a full understanding of how the cell temperature can be monitored using acoustic ToF analysis, it is important to study how the acoustic signal is influenced by the SoC of the cell. Results summarized in Fig. 3 have shown that, as expected, the material changes with SoC influence the material properties, which in turn affect the acoustic signal. In order to use ultrasonic methods to determine the cell temperature while cycling a full understanding of how the signal varies with SoC is required.
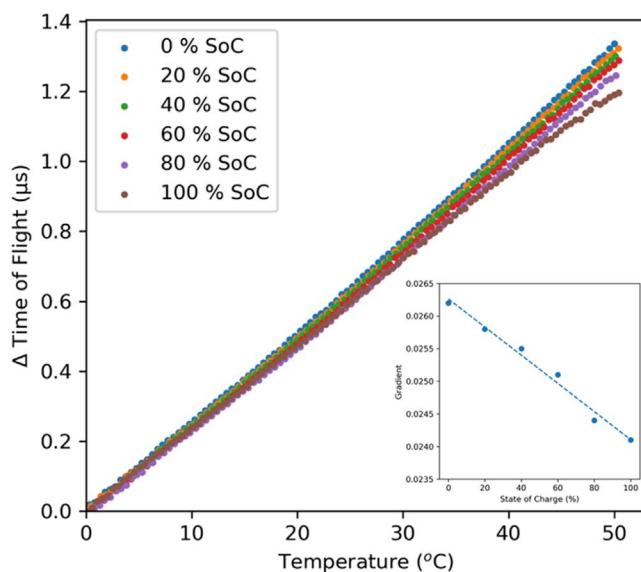

Figure 3. The effect of SOC on the relationship between the time-of-flight and temperature. Insert; the variation of trendline gradient with SOC/capacity.

To determine the effect of SoC on the acoustic signal a 210 mAh pouch cell was charged at a constant current of C/5 before the voltage was held at 4.2 V until the current dropped to 10.5 mA. At this point, the cell was then discharged at a constant current of C/5 until the voltage reached the manufacture's cut-off voltage of 2.75 V. During this charge-discharge cycle the acoustic signal was monitored, the results obtained from this test are summarized in Fig. 4.

The change in the acoustic signal as the voltage (Fig. 4c) and applied current (Fig. 4d) changes across the cycle is shown in
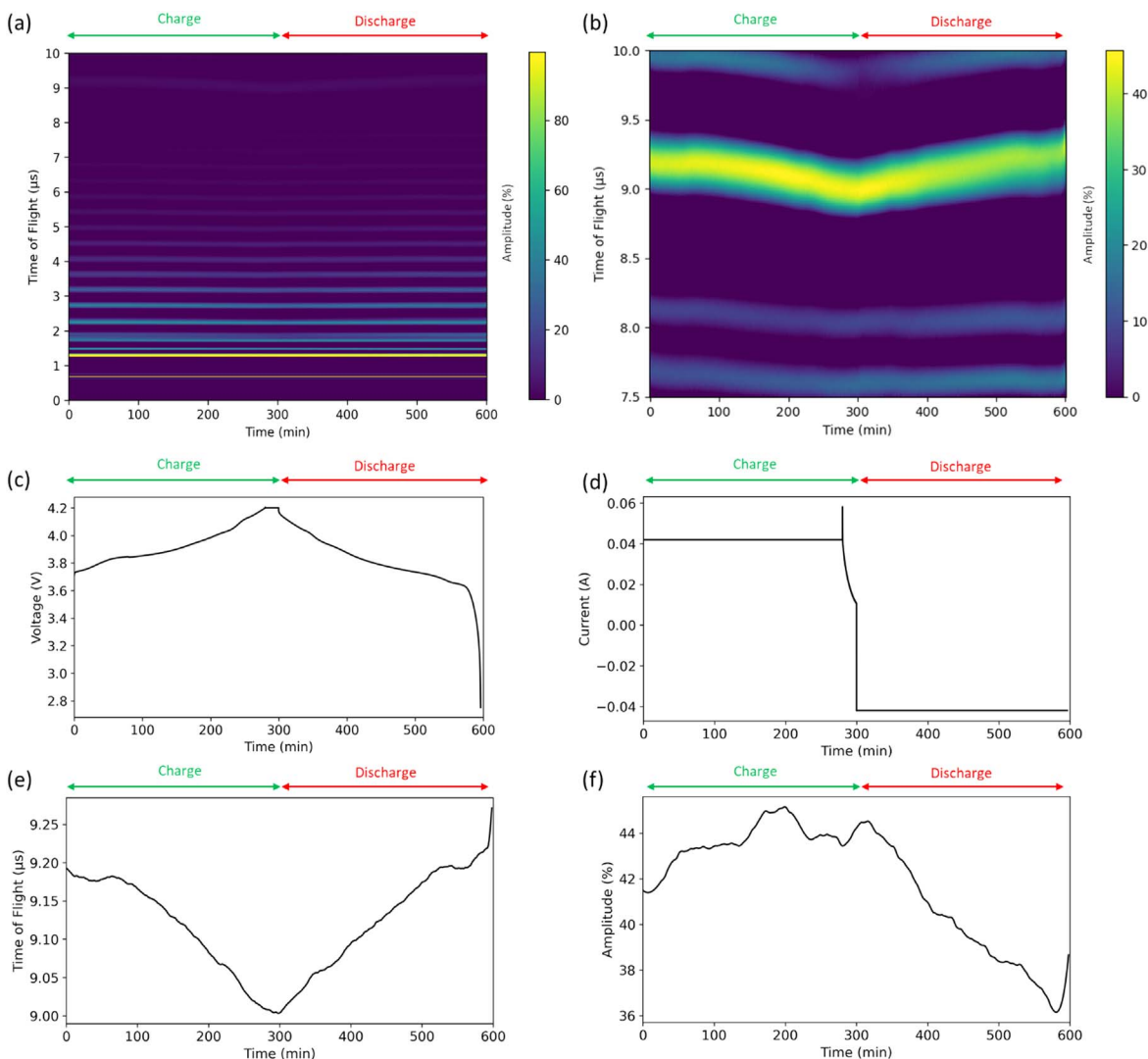
Figure 4. A single charge-discharge cycle of a 210 mAh pouch cell and the resulting change in the acoustic signal. (a) the change in the acoustic waveform at a low gain (b) the change in the first echo peak recorded at high gain. (c) the cell voltage, (d) the applied current, (e) the ToF of the first echo peak, (f) the change in amplitude of the first echo peak (note: due to the lower resolution of the amplitude measurements the data has been smoothed before plotting).

Fig. 4a. As the cell is charged and discharged a change in ToF is evident. As with the temperature changes, these variations in peak position become more evident as the peak's initial ToF increases. These changes are most evident with the "first echo" peak, as such readings at a higher gain were recorded concurrently allowing for a more detailed study of how the "first echo" peak varies across the experiment, these results are shown in Fig. 4b. The ToF and amplitude of the "first echo" peak are plotted in Figs. 4e and 4f respectively.

As the cell is charged and the voltage increases the ToF of the "first echo" peak gradually decreases. As the cell reaches the CV stage of charging the ToF also begins to level off. Once discharge begins the ToF increases accordingly with a more rapid shift at the end of the discharge step where the voltage undergoes the largest change. As the cell is charged, a range of changes are occurring within the anode and cathode of the cell. Over the course of a charge the LCO cathode has been reported to expand by 1.8% and the graphite anode 5.8% resulting in an overall increase in the thickness of the cell (*ca.* 2.4% including inactive materials).[31] If the cell expansion was the only property affecting the ToF of the "first echo" peak then the increased thickness would result in a longer path length for the signal to travel resulting in an increased ToF and reduction in amplitude. Generally speaking, the opposite of this is observed in the experiment with an overall decrease in ToF and

increase in amplitude as the cell is charged (Figs. 4e and 4f), similar results were observed in acoustic guided wave studies conducted by Ladpli et al.[12] and transmission studies reported by Knehr et al.[33] This demonstrates the complexity of the processes occurring within the cell and illustrates the power of acoustic measurements to provide more information than that generally achieved by thickness measurements that acoustic systems are often applied to.

As the cell is charged, the LCO cathode is delithiated and the graphite anode lithiated. These processes not only result in a change in thickness of the electrode materials but significant changes in the physical properties of the materials such as elastic moduli and densities. While the process is occurring the electrodes are subjected to stresses and strains associated with the processes taking place, these too, have been shown to influence the speed of ultrasound through a material.[14]

While the thickness of the cell will have an effect on the ToF of the "first echo" peak, the effect is dominated by other material property changes occurring within the cell. For example, when graphite is lithiated in the charge step the graphite expands by $\sim 7\%$; however, this expected increase in ToF for this change is likely dominated by the *ca.* 300% increase in modulus[34] which results in an increase in wave propagation speed and a reduction in ToF. Changes in the density of the materials also occur and will contribute to the process. While many processes play a role in altering the

speed of the wave upon charging, these are dominated by the processes which increase the velocity. All of the material property and thickness changes occurring will also affect the amplitude of the first echo with all factors influencing the complex attenuation processes occurring.

In general, as the cell is charged the amplitude of the first echo peak gradually increases and as the cell discharges the amplitude decreases. There are, however, several notable deviations from this trend. A maximum is reached at *ca.* 200 min with the amplitude only beginning to increase again once the CV step is reached. In addition to this maximum in the charge step, there is also a deviation at the end of discharge where an increase in amplitude is observed as the voltage rapidly drops. Due to the lower resolution of the data collection of the amplitude compared to the ToF, a smoothed data plot is shown in Fig. 4. Equipment with a higher amplitude resolution is required to gain a more detailed insight into the effects of SoC on signal attenuation.

Although not as obvious as the changes observed for the "first echo" peak, all peaks undergo the same general trends in ToF shift over the course of the charge-discharge cycle (See SI Fig. 1). A decrease is observed for all during charge with an increase during discharge. The relative shift in ToF is reduced as the initial peak position is lower, this is consistent with what would be expected from reflections occurring nearer the surface of the cell. Reflections from deeper within the cell (peaks positioned at higher initial ToFs) must travel through more of the cell before being reflected; as such, the effects of changing material properties (e.g. density or elastic moduli) will be magnified since they must pass through a greater thickness of the material undergoing change.

Repeatability of acoustic readings under continuous cycling.—
With the "first echo" peak showing the largest changes due to both temperature and SoC, in combination with the fact it can give information on the cell as a whole, this peak is the focus of the remainder of the study. Clear shifts in ToF were observed over the course of a single cycle (Fig. 4). To demonstrate the repeatability of the results and determine the magnitude of the cycle-to-cycle variation the charge-discharge cycle was repeated multiple times. Each cycle should theoretically result in the same changes in material properties unless degradation effects are significant. As such, the change in the speed of sound through the cell and resulting ToF shifts should be repeatable from one cycle to the next if all cycling conditions remain constant. With the cycle-to-cycle variability determined, it should then also be possible to determine what shift in ToF would constitute a significant change in the SoH or temperature of a cell. To demonstrate the repeatability, a 210 mAh cell was subjected to five charge-discharge cycles at a rate of C/5 while acoustic measurements were being collected. The results from these tests are summarized in Fig. 5. Figure 5a shows the behavior of the first echo peak across the course of the test as a colourmap plot with the applied current and resulting voltage change shown in Fig. 5b. The changes in amplitude were observed to be similar from cycle-to-cycle with a maximum amplitude observed at end of CV charging and the start of discharge.

The change in the ToF of the "first echo" peak across the five test cycles is shown in Fig. 6, across all five charge steps a similar profile is observed. The largest deviation was measured for the first charge step (Blue line, Fig. 6a). During discharge, all steps display similar ToF profiles (Fig. 6b); however, there is a deviation in ΔToF for the first discharge. With the final four charge-discharge cycles showing little variation, it suggests that a new unequilibrated cell that has just begun being cycled undergoes slightly different stresses and strains during the first cycle and has a slightly different temperature profile (Fig. 5c). The introduction of a sufficiently long rest step between cycles would likely resolve this difference. Cell relaxation between cycles is discussed in more detail later. There is also a slight difference between charge 4 and charge 2, 3 and 5, this may be related to some differences in the temperature profile observed for this cycle (see Fig. 5c), the remaining cycles show a relatively good

consistency and the deviation for cycle 4 is relatively small compared to the total ToF change. A ToF shift of *ca.* 0.35 μs is observed for both the charge and discharge with a range of ± 0.026 μs including the first cycle or ± 0.015 μs excluding cycle one. Based on these results we can suggest that any changes in ToF greater than this value at any point during cycling are likely related to significant cell damage (significantly larger than cycle-to-cycle degradation) and/or temperature changes occurring within the cell much larger than would be expected for this cycling rate. This potentially allows for the early detection of cell damage and heating before a cell may undergo significant heating, damage or enter thermal runaway allowing for mitigation strategies to be applied.

Effect of cycling rate on the acoustic signal.—
As demonstrated, the material property changes occurring during the charge-discharge cycle of a Li-ion pouch cell have a repeatable effect on the acoustic signal, particularly the ToF of the first echo peak. To use the position of this peak to determine the SoC and potentially detect any unexpected cell heating or damage, a potentially significant indicator for BMSs, it is important to understand how the rate at which a cell is charged and discharged will affect the acoustic signal. Thus far, the majority of published literature focuses on a single rate of charge and discharge, normally relatively low to minimize stresses and strains and reduce temperature effects. Recently, Robinson et al. published a study looking at the effects on high cycling rates, some outside the manufacturer's recommended specification, on Li-ion pouch cells using ultrasound.[20] The study focused on monitoring the stresses and strains in electrode layers close to the surface of the pouch cell and found significant differences in the acoustic response between different C-rates. Work by Popp and coworkers also investigated the effect of C-rate on ultrasonic ToF using a guided waves method and found different ToF changes for each rate tested.[17]

For this study, the focus is on the entire cell and to determine what effect the C-rate has on the acoustic response of the cells under test, to understand how this technique may later be applied to monitor real-world systems where the rate of changes of SoC are irregular and generally much higher than the low C-rates regularly reported for acoustic studies. This will provide an understanding of whether it is necessary to account for the rate of charge and discharge when calculating the SoC based on acoustic measurements. The influence of C-rate was determined by repeating the cycling experiment shown in Fig. 5 at two further C rates, C/2, and 1 C. The results from these tests are summarized in Figs. 7 and 8, respectively.

A similar profile is observed for all tested cycling rates with a decrease in ToF during charging and an increase during discharge. These changes are observable in the acoustic signal with a distinct "kink" in the reducing ToF as the cell is charged. The position of this matches up with the transition from the CC to the CV step and is presumably related to the changes in the stresses on the electrode as well as changes in the rate at which the electrochemical processes are occurring and the resulting temperature effects. This "kink" in the ToF of the first echo peak is, as expected, not present during discharge due to the lack of a CV step and the associated transition.

In addition to the change in the shape of the charge ToF and amplitude profile, there is an obvious change in the magnitude of the temperature changes the cell undergoes under differing C rates. As would be expected as the rate of charge and discharge is increased the temperature variation also increases with a variation of *ca.* 5 °C observed over the course of a cycle at 1 C compared to *ca.* 1 °C seen at C/5.

To further assess the effects of the C-rate on the acoustic properties Fig. 9 shows a comparison of the ΔToF measured at each C-rate, a complete discharge-charge cycle is shown for each rate. From Fig. 9a it is clear that there is a large difference between the change in ToF with each C-rate. Even when the differing cycle times are considered there is still an obvious difference in the height of each of the peaks, indicating a difference in the ΔToF based on
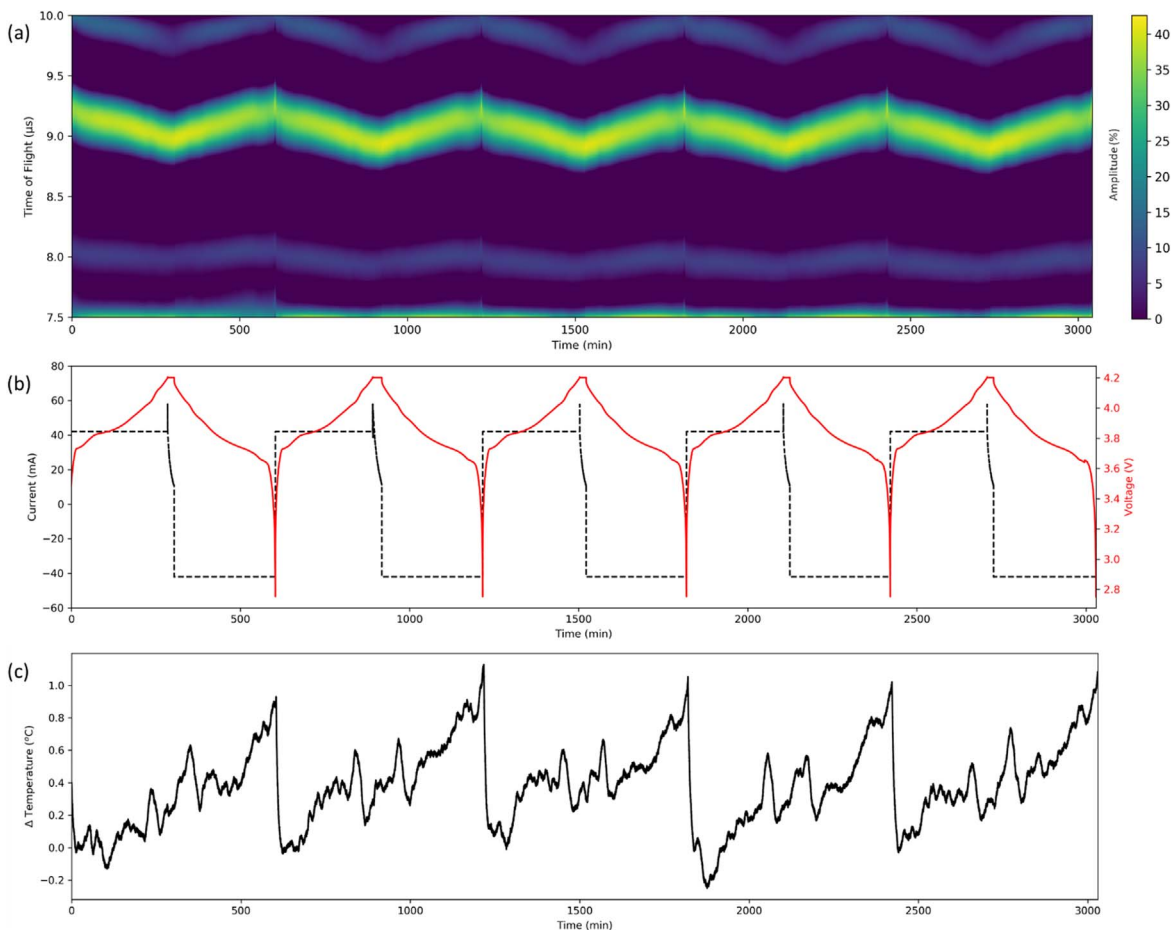
Figure 5. C/5 cycling of a 210mAh pouch cell. (a) A colourmap plot showing the changes in amplitude (colour) and time-of-flight (position on the *y*-axis) of the first echo peak versus time (5 cycles, *x*-axis). (b) the applied current and resulting voltage changes over the course of the cycling and (c) the change in cell temperature as the cell was cycled at room temperature.
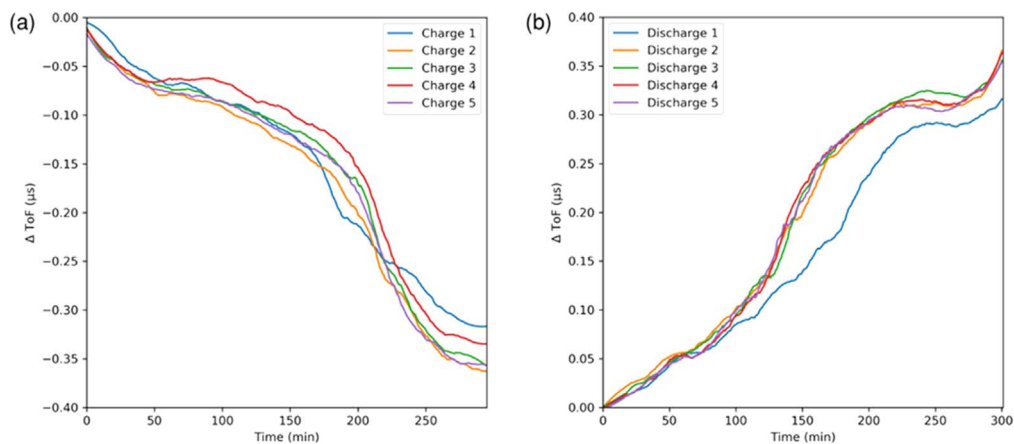

Figure 6. The change in ToF of the first echo peak as a 210 mAh pouch cell is cycled five times at C/5 (a) change in ToF as the cell is charged (b) change in ToF as the cell is discharged.

the C-rate. If the changes in ΔToF are based purely on the material properties of the cell and the thickness changes that occur when the electrodes are lithiated and delithiated it would be expected that the ΔToF would be similar regardless of the rate at which the cell is charged or discharged, indicating the influence of other factors.

To more accurately compare the ToF changes and account for the differing times taken for each discharge-charge cycle the discharge of the cell at each C-rate was plotted against the depth-of-discharge,

Fig. 9b, the charge is omitted for clarity and is shown in Fig. 10c. From this plot, it is clear that although the general trend is similar for all C-rates, the extent of the change in ToF is dependent on the rate of discharge. At all rates there is a relatively linear relationship between the ToF and DoD between 0 and 75%, at this point, there is a slight drop in ToF followed by another increase. The depth of this dip decreases as the rate of discharge increases with 1 C showing a more linear profile relative to the C/5 discharge.
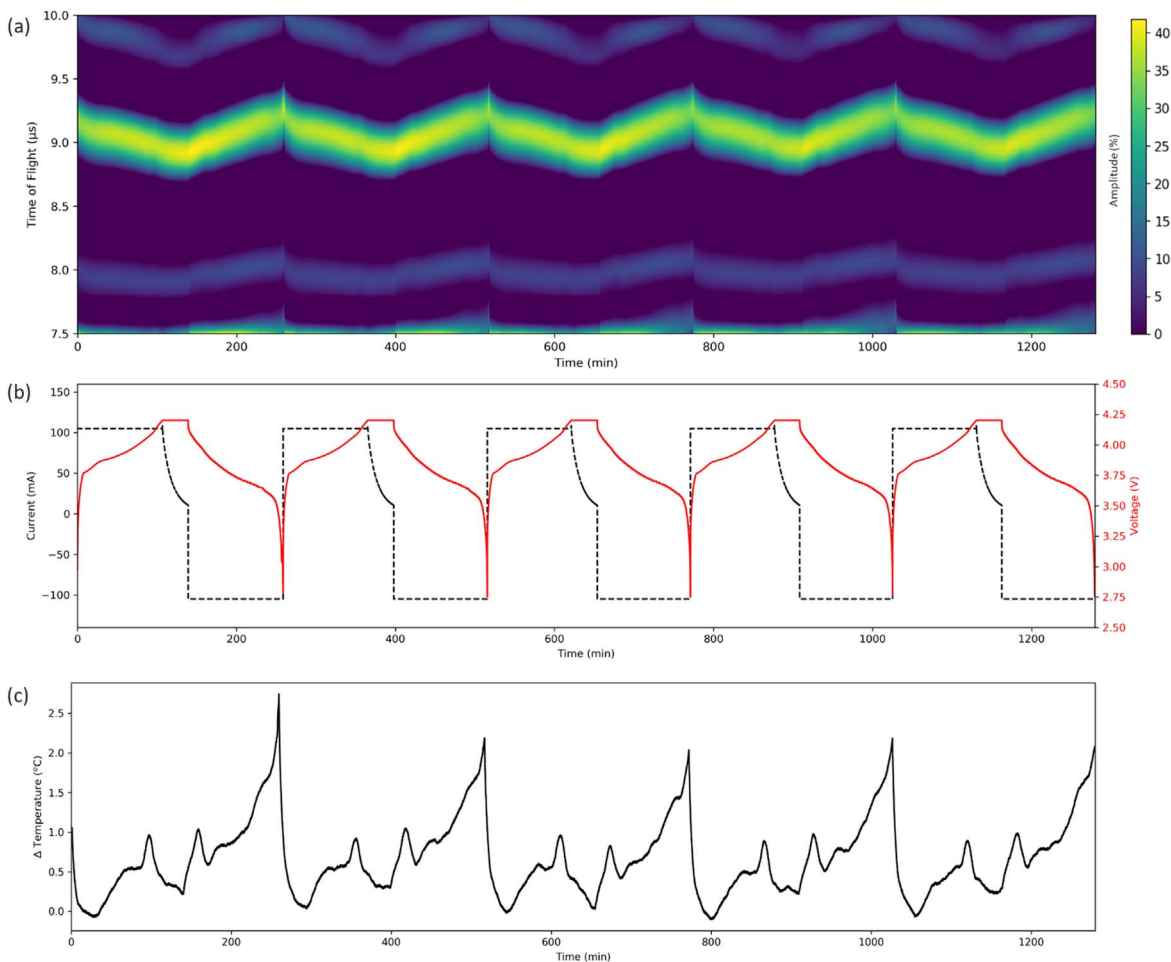
Figure 7. Five cycles at C/2 of 210 mAh pouch cell. (a) colourmap illustrating the change in position and amplitude of the "first echo" time-of-flight peak (b) the voltage change and applied current (c) cell temperature variations while being cycled.

As illustrated in Fig. 2, the temperature can have a significant impact on the ToF of the "first echo" peak, the large difference in temperature change at each rate (see Fig. 5(c), Figs. 7c, and 8c) is likely to play an important role in the different ΔToF observed. This illustrates the importance of understanding how a cell operates at different C-rates before this technology can be employed in "real world" conditions and utilized in BMSs where different and relatively high C-rates are required. To either monitor the SoC or the temperature of the cell using ultrasound, the effects of each on the acoustic signal must be decoupled.

Decoupling the effects of temperature.—The effect of SoC on the ToF of the "first echo" peak during a single C/2 discharge-charge cycle is shown in Fig. 10b where the ΔToF has been plotted against the DoD of the cell. Here it can be seen that at lower DoDs, higher SoC, the relationship is relatively linear with a small bump or deviation at *ca.* 20% DoD. Above this value, hysteresis is observed with the largest deviation between charge and discharge ToF at *ca.* 80% DoD. The ΔToF then converges again at 100% DoD. Although a similar trend in ToF shift is observed at all C-rates (See Fig. 10c), the extent of hysteresis, and total ΔToF vary considerably.

This hysteresis and the deviations from linear may in part be related to the temperature of the cell, Fig. 10a shows how the temperature of the cell varies with DoD during charge and discharge at C/2 and shows that the cell temperature is not only dependent on the cell SoC but also if the cell is being charged or discharged. There is a relatively small increase in temperature at *ca.* 20% DoD which corresponds to the location of the small bump/deviation away from linearity in the ΔToF (Fig. 10b). It is also noteworthy that the largest

deviation in cell temperature at *ca.* 80% DoD corresponds with the largest hysteresis observed in the ΔToF curves.

Using an equation based on the plots shown in Fig. 3 and the cell temperature measured using the surface thermocouple it is possible to determine the ΔToF that can be attributed to the changes in cell temperature (SI Fig. 2). These temperature-related changes in ToF can then be subtracted from the measured ToF to give the "temperature compensated" ToF. The values of the temperature compensated ToF should be independent of the cell temperature variations and instead dependent solely on the material property changes associated with the SoC changes occurring during charge and discharge. Figure 10b shows how the temperature compensated ΔToF compares to the original, measured ToF data. With the temperature-related ΔToF accounted for there is a significant reduction in the hysteresis observed; however, it is still present, suggesting that this effect is not entirely down to the difference in cell temperature but potentially also the processes occurring within the cell that lead to the observed difference in temperature. The small bump at *ca.* 20% DoD, in contrast, is removed when the temperature is accounted for, suggesting that this slight deviation from linearity is related mainly to the changes in cell properties due to temperature.

When the ΔToF plots of all three C-rates are compared after compensation for temperature effects (Fig. 10d) the data is more consistent across C-rates. Each of the discharge-charge cycles shows the same linear trend and same change in ΔToF in the DoD region of *ca.* 0–80% regardless of C-rate. This is a strong indication that the deviations observed in this region for the non-processed data (Fig. 10c) are due to the different temperature shifts observed at
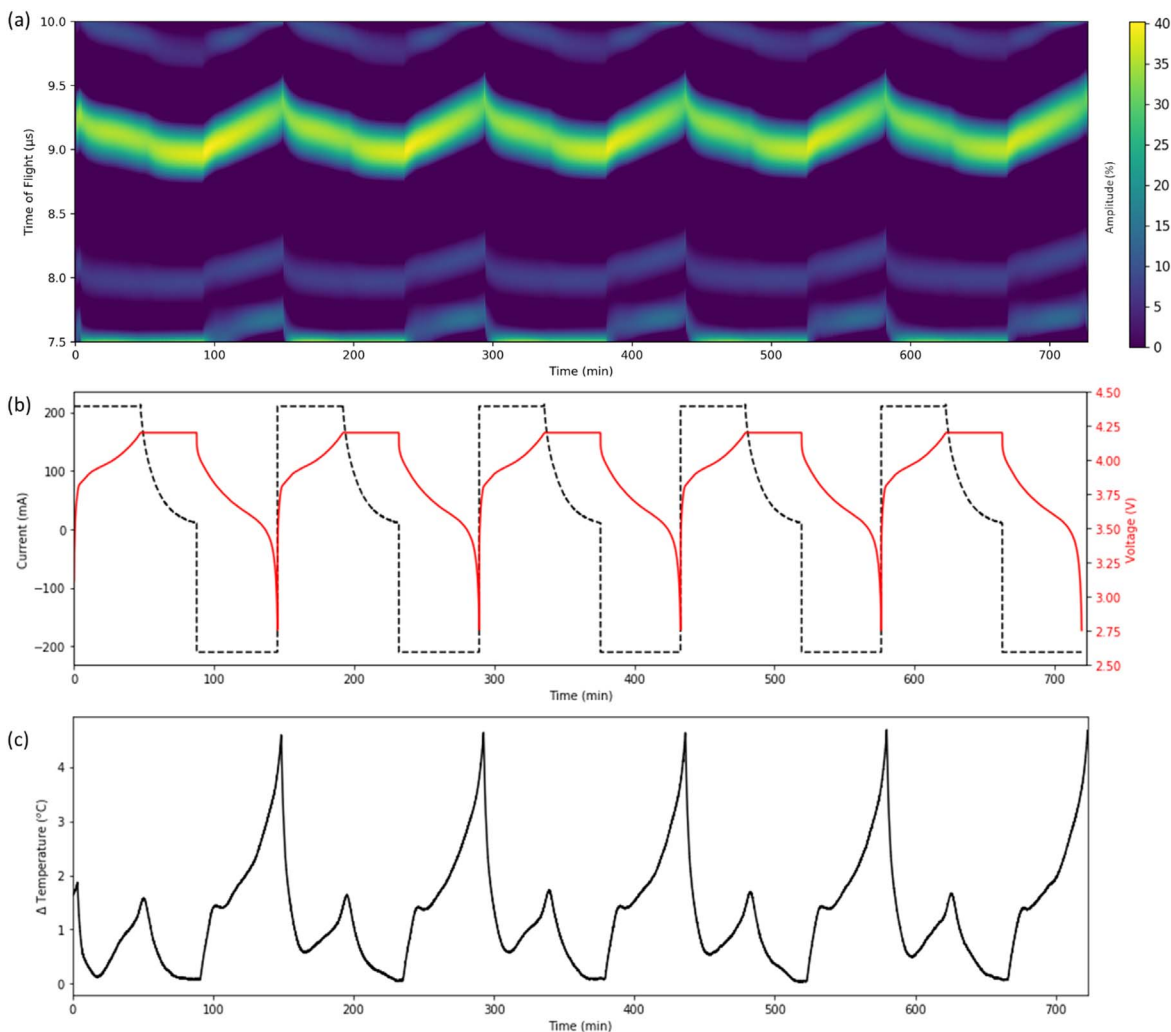
Figure 8. Five cycles of a 210 mAh pouch cell at 1 C. (a) colourmap illustrating the change in position and amplitude of the "first echo" time-of-flight peak (b) the voltage change and applied current (c) cell temperature variations while being cycled.
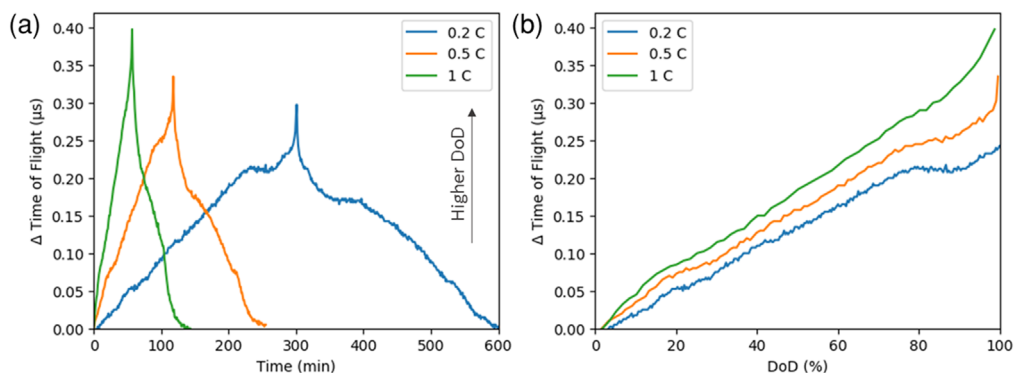

Figure 9. (a) The difference in ToF shift for the first echo peak at different discharge and charge rates. Cell charged first followed by discharge (b) ToF shift of the first echo peak normalised to the depth of discharge of each cell.

different C-rates rather than differences in the material properties resulting from different C-rates. When this is accounted for, the same SoC results in the same change in ToF due to the same changes in material properties occurring within the cell. Despite the good agreement observed in the 0%–80% DoD range, there is still some deviation in the lowest SoC (highest DoD). These effects are greatly reduced when the effects of temperature are taken into account. Studies conducted on the thickness of lithium-ion batteries under

operation have shown a similar hysteresis between charge and discharge in this region of the cell's SoC and are related to the difference between lithium-ion insertion and extraction processes in the graphite anode.[35,36] At lower currents the intercalation stages through which the lithiated graphite passes are dependent on whether the cell is being charged or discharged. Thickness measurements indicate that when discharging the anode passes through additional intercalation stages not present during charge. Work reported thus
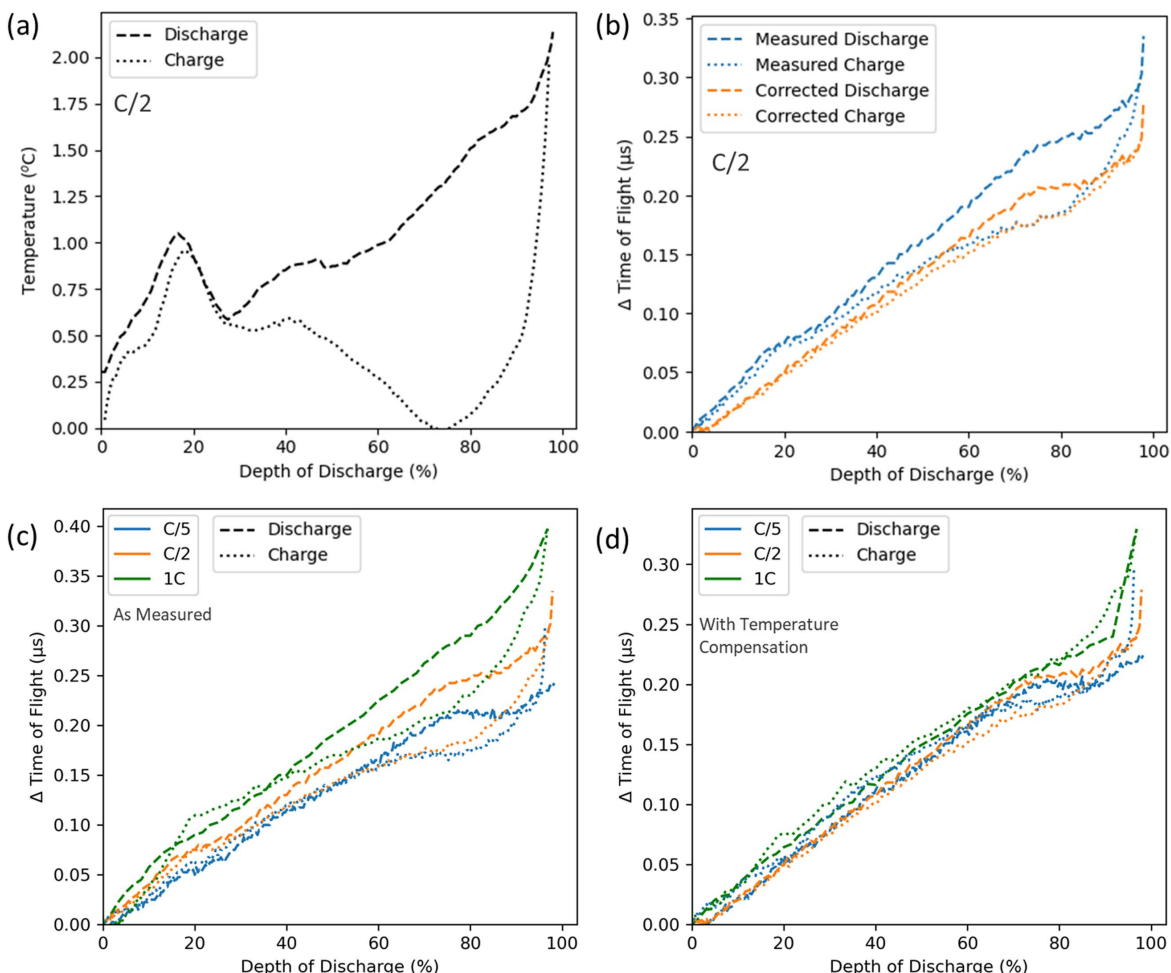
Figure 10. (a) The variation of cell temperature during charge and discharge of a 210 mAh pouch cell cycled at C/2. (b) the ToF shift observed for a 210 mAh cell charged and discharged at C/2 as recorded (blue) and with the effect of temperature compensated for (orange). (c) The ToF shifts observed for a 210 mAh pouch cell cycled at several different C rates, as recorded and (d) with the effect of temperature compensated for.

far indicates that the different material properties for differing anode properties would likely be detectable using ultrasound analysis and may offer an explanation for the hysteresis observed. The intercalation stages of the graphite are current dependent with higher currents observed to reduce the hysteresis,[36] a similar trend is observed in this work with the ToF changes during a 1 C charge-discharge showing little evidence of hysteresis when compensated for temperature relative to the C/5 results, Fig. 10d. Similar hysteresis behavior attributed to the same changes in intercalation stages has also been observed with the OCV of graphite half cells.[37]

As shown in Fig. 10d, the ToF shift related to the changing SoC is consistent regardless of C-rate. The difference between the ΔToF observed for the uncorrected measurements is determined by the difference in temperature between the cells at different C-rates. Since this change in ToF is proportional to the temperature the proportion of the DToF contribution from the temperature changes with C-rate, for 1 C 31% of the change in ToF is related to temperature whereas for 0.5 and 0.2 C this values drops to 18% and 10% respectively.

The ability to decouple the effect of temperature allows for the changes in material properties to be studied in more detail using ultrasound. An example of one area where this may be particularly important is at the end of the cell cycling when the discharged step is finished and the cell is allowed to relax. To further study what is happening during this "relax" phase, a pouch cell was charged at 1 C CC, held at 4.2 V until the current dropped to 0.0105 A then discharged at 1 C until 2.75 V. Once this voltage was reached the

cell was allowed to relax while voltage, temperature, and ultrasound readings were recorded. A summary of the results obtained from this experiment is shown in Fig. 11. At the end of discharge, the cell is at its highest temperature. As soon as the current is reduced to zero and discharge is stopped the cell begins to rapidly cool. As the cell is cooling in this "relax" period there is a concurrent drop in the observed ToF. With the large drop in temperature and ToF occurring it is not possible to determine what exactly the cause of the ToF shifts are. When the effect of temperature on the ToF is taken into account (Fig. 11d) it is shown that a larger portion of the ToF shift was, as expected, related to the temperature of the cell with a divergence of the corrected and uncorrected ToF as the temperature of the cell increases. With the effects of temperature compensated for there are still observed shifts in ToF observed as the cell "relaxes." This suggests that, as indicated by the voltage, material property changes not necessarily caused by temperature, are occurring. Previous works have shown similar shifts in ToF for peaks at lower initial times-of-flight relating to the internal structure of the cell.[16] These are suggested to be related to the un-stiffening and relaxation of the electrode. Interestingly, while Robinson et al.[16] reported a C-rate dependence on the extent of this observed relaxation at high C-rates, no obvious influence of C-rate on this relaxation period was observed when the temperature is compensated for (See SI Fig. 3). This may well be related to the lower C-rates reported in this study. Another potential contributing factor may be temperature gradients within the cell. Previous work has shown that significant temperature gradients can be present within cells while they are cycling and, as such, the
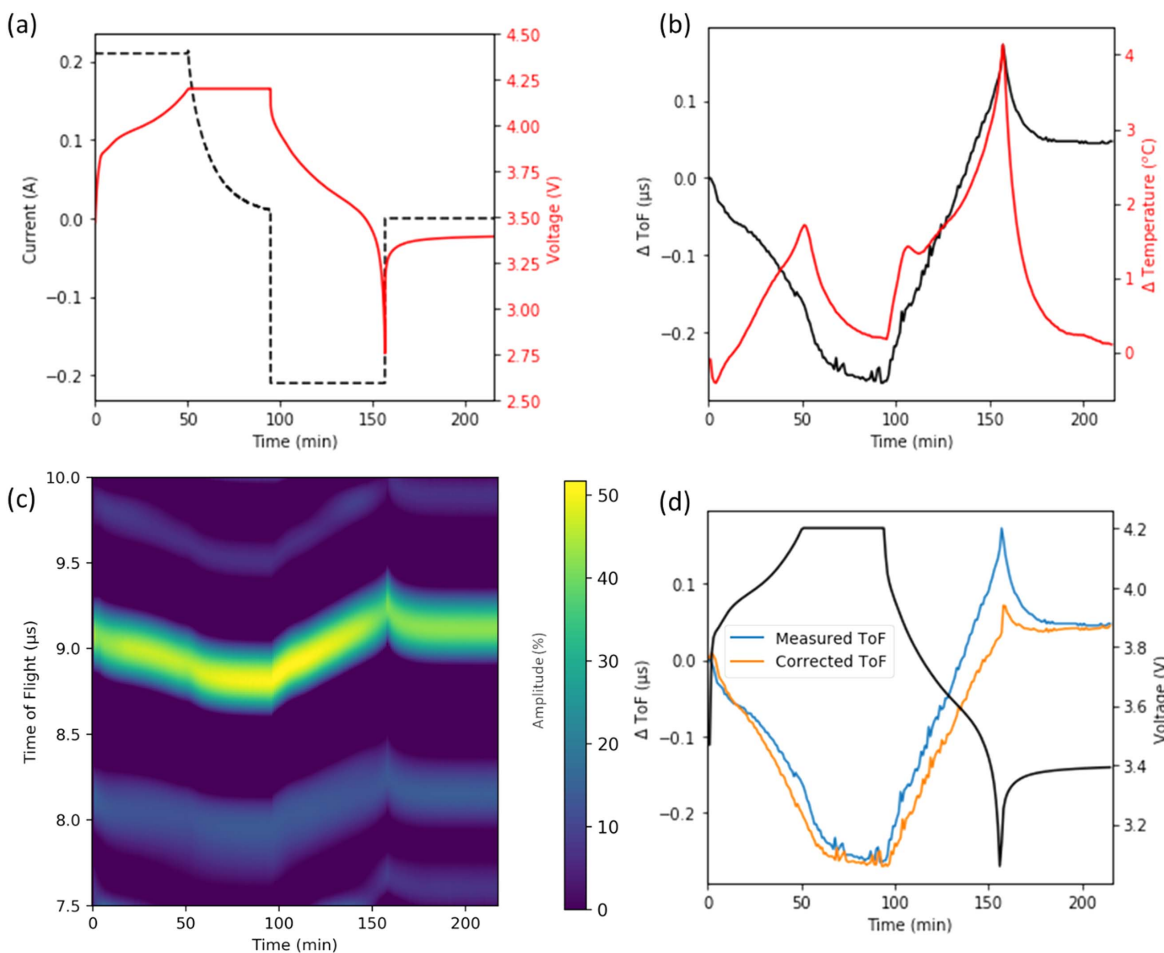
Figure 11. Ultrasonic investigation of cell relaxation after cycling (a) the applied current and voltage profile for a 1 C charge and discharge of a 210 mAh pouch cell with following relaxation period. (b) the variation in temperature and ToF across the test (c) the variation of the position and intensity of the first echo peak (d) the difference in ToF variation with and without temperature effects compensated for, superimposed upon the voltage profile.

temperature of the thermocouple may not be representative of the whole cell and may introduce small errors. For a cell of the size used in this study, these effects should be minimal, however, when larger cells are used the temperature gradient may be more significant and result in a larger impact of these effects.

Estimation of cell temperature and SoC based on ultrasound measurements.—When the cell temperature is known, its effect on the ToF can be accounted for and the SoC monitored using ultrasound as shown in Fig. 10. With the effect of temperature removed, the change in ToF is similar regardless of the C-rate. Therefore, if the SoC of the system is known the opposite can be done and the effect of SoC on ToF can be removed and the temperature tracked using ultrasound, illustrating the power and flexibility of the ultrasound technique.

If neither the SoC nor temperature are known, an indication of when a cell is operating outside of its normal parameters can still be obtained by monitoring the ToF of the first echo peak. When a cell is operating within parameters, i.e., without significant degradation and at expected temperatures, then the ToF would be expected to remain within a certain ToF range. If the ToF of an operating cell leaves this range it is an indication that the cell has become too hot, damaged or degradation is occurring and corrective action should be taken. To determine how accurately the cell temperature and SoC can be monitored using an ultrasonic method, predicted values, based on the assumptions above, were compared to the measured values. The results from these tests are summarized in Fig. 12.

The predicted SoC was calculated by first compensating for the effect of temperature, with these effects removed the remaining changes in ToF can be attributed to the material property changes associated with the SoC. To predict the SoC based on the ToF change, the temperature compensated ToF was plotted against the measured SoC, the data were then fitted and an equation that could be used to predict the cell's SoC based on observed ToF was obtained (SI Fig. 4). The equation was derived from the C/2 test data since this was in the middle of the rate range studied. The same equation derived from the C/2 data was used for all calculations regardless of C-rate. Figures 12a, 12c, and 12e show the resulting SoC estimations for C/5, C/2, and 1 C, respectively. Irrespective of the C-rate at which the cell is operating, a good agreement between the measured SoC and that predicted by ultrasound measurements is observed. The largest deviations from the measured values are at lower SoC (0%–20%) in the region where the largest hysteresis is observed in ToF (Fig. 10) due to the cell possessing slightly different material properties at one SoC depending on whether the cell is being charged or discharged. These deviations are less significant at higher C-rates where, as observed in Fig. 10, the material properties are more similar during charge and discharge. A combination of ToF shift with other parameters such as OCV may allow for a more accurate prediction of SoC than either technique can provide individually. These results show that the SoC of a cell can be determined from ultrasonic measurement regardless of the C-rate they are operating under providing that the temperature of the cell is accounted for.
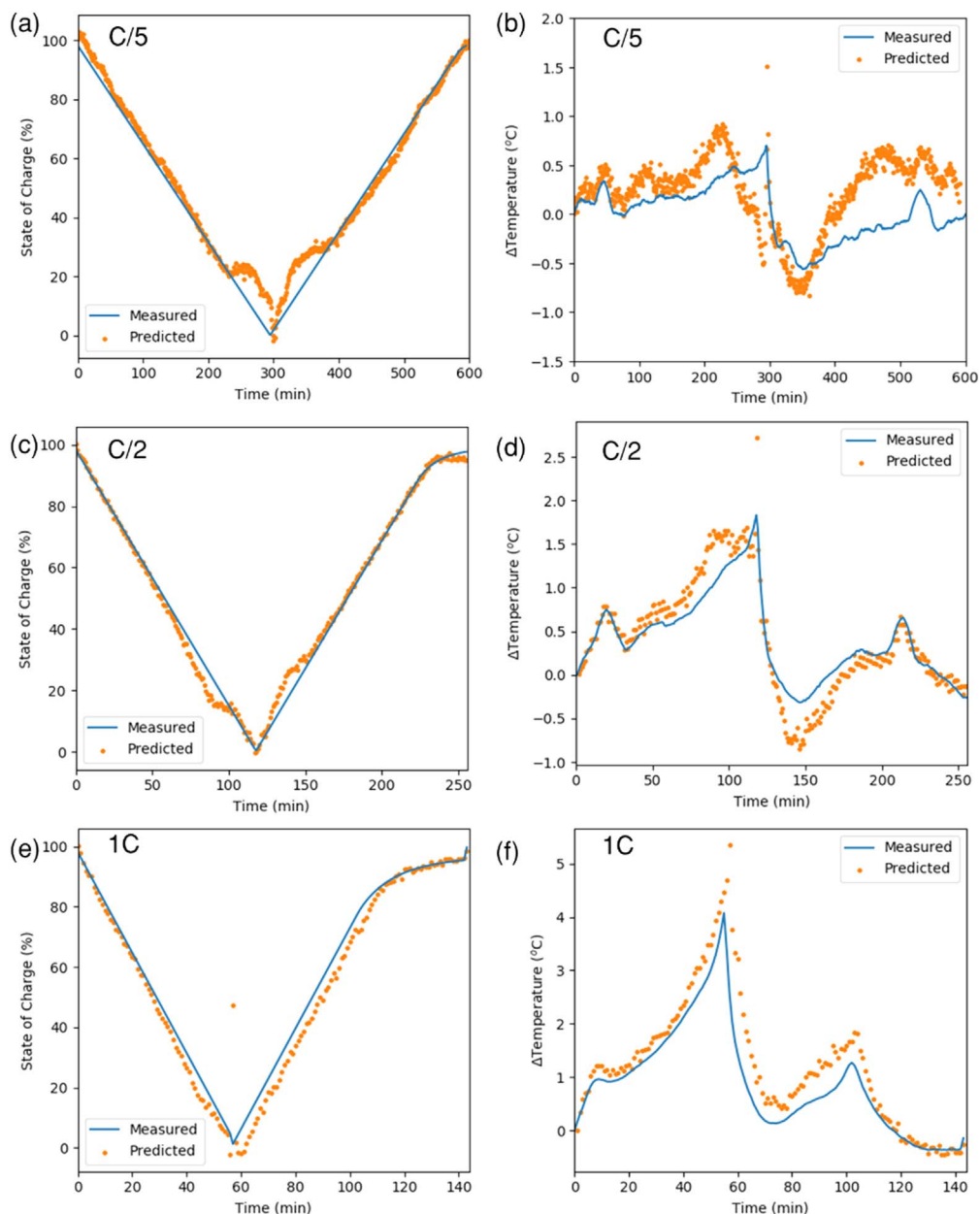
Figure 12. The measured SoC and temperature compared with that predicted by the decoupled ToF changes for C/5 (a) and (b), C/2 (c) and (d) and 1 C (e) and (f).

To predict cell temperature based on ultrasonic measurements, the effect of SoC is first compensated for, this is achieved by removing any ToF shift associated with the measured SoC change (SI Fig. 5). With the effect of SoC on ToF removed, an equation based on the plot shown in Fig. 3 was used to predict the temperature of the cell (SI Fig. 2), the results from this study are summarized in Figs. 12b, 12d, and 12f. A relatively good correlation between predictions based on ultrasound measurements and the cell's actual temperature is observed at all C-rates, even C/5 where temperature variations are relatively low. Where the ToF changes are larger due to larger temperature changes, the magnitude of error in decoupling makes the prediction of both SoC and temperature more accurate.

Based on the results shown in Fig. 12, ultrasonic measurements are well suited for implementation in BMSs where information on SoC and temperature is vital for the safe and efficient operation of battery modules. Ultrasonic measurements such as those reported here offer the potential for a low-cost technique with a simple model

requiring very little computational power to predict SoC. In addition to SoC and temperature, the ultrasonic measurements can indicate the SoH of a cell and warn if a cell begins to rapidly degrade or if large temperature gradients are present within the cell. While Fig. 12 demonstrates the ability of this ultrasound technique to monitor the SoC irrespective of the C-rate at which the cell is operating, this is still unrealistic for real-world applications such as EVs. In real-world applications, the current draw is rarely constant for any significant period with demand varying greatly depending on whether the vehicle is accelerating or maintaining a constant speed. In addition to this, the regenerative braking present in EVs means that the cell quickly switches between charge and discharge at non-constant rates. For this technology to be applied in these situations the system must be able to maintain its ability to predict SoC even under these conditions rather than the low C-rate galvanostatic operation thus far reported for ultrasound measurements. To determine the ability of the technique to operate under these
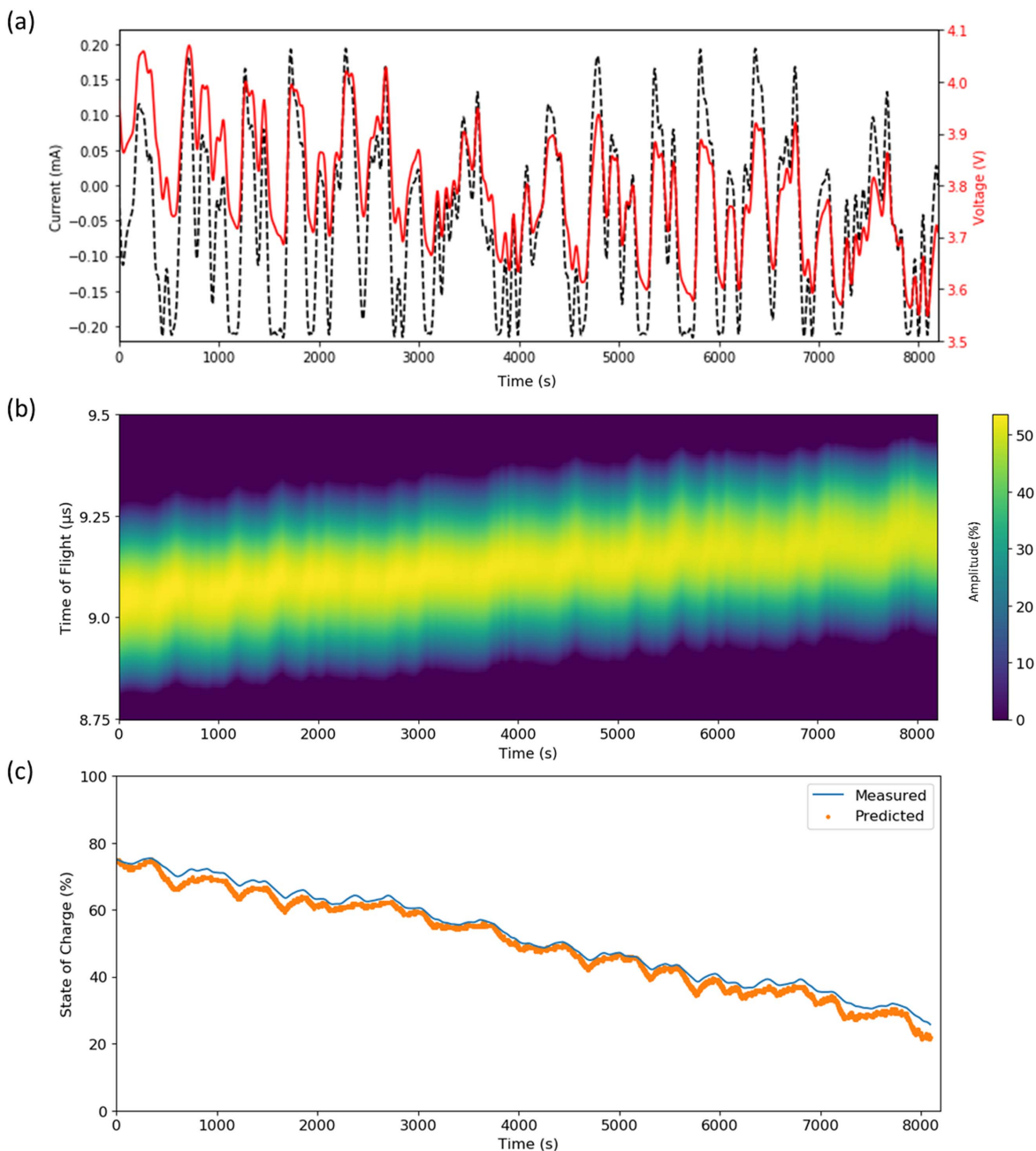
(a)

(b)

(c)

Figure 13. (a) The current applied during the drive cycle test and resulting voltage. (b) The variation in position and intensity of the first echo peak across the drive cycle test. (c) the measured change in SoC and the SoC value predicted by the ToF of the first echo peak.

demanding conditions a drive cycle test was run while ultrasonic measurements were recorded. The results from this test are shown in Fig. 13.

As shown in Fig. 13b, the acoustic signal collected at 0.5 Hz responds rapidly to the changes in the cell state-of-charge as it is subjected to the drive cycle (Fig. 13a). Over the course of the test, the cell is slowly discharged from its initial SoC of 75% to ca. 25%. This change in SoC results in an overall increase in ToF of the first echo peak (Fig. 13b). When the cell temperature is compensated for the ToF can be used to predict the cell SoC using the same equation used to generate Fig. 12; the predicted values are plotted in Fig. 13c along with the measured SoC. Although some slight deviations are observed, overall, the predicted values match well with the measured values demonstrating the ability of this ultrasonic technique to monitor the SoC of cells under simulated drive cycle conditions.

The results covered in this study show the promise of the technique to be applied in BMS systems, however it should be stressed that these studies have been conducted on a relatively small, fresh cells. In order for this to be applied to real world applications the effect of SoH on the time of flight must also be considered in addition to potential thermal gradients that may be observed on larger cells.

Conclusions

To this point, the use of ultrasound to monitor the performance of batteries has mainly been limited to low C-rates and galvanostatic operation, while these works have been of vital importance in developing the technique, a deeper understanding is required of how the C-rate of operation and the temperature of the cell affect the

ultrasound measurements. This work has demonstrated the ability to decouple the effects of temperature and material property changes due to SoC, allowing for either the cell temperature or the cell SoC to be predicted in *operando* using ultrasound analysis regardless of the C-rate the cell is being operated at. Drive cycle tests have shown that this technique can be applied in "real-world" situations where the cell is rapidly switching between charge and discharge and the C-rate is being varied.

The ability to monitor either of these two variables using a non-destructive and relatively low-cost process takes this ultrasound technique another step towards its potential use in "real world" applications and BMSs, not only to monitor SoC and temperature, but to give additional information about any potential damage occurring that is currently undetectable by the majority of techniques implemented in BMSs to date. These studies have been conducted on relatively small cells in terms of size and capacity and as such further work is required to determine how effective these processes will be on larger format cells. Despite this it is a promising step towards utilisation in BMSs. Due to the nature of the technique, it is not only surface-sensitive but should also be able to rapidly detect any changes in temperature occurring within the cell or any significant temperature gradients, something not easily achieved with current techniques, giving additional time to potentially stop thermal runaway and improve the safety of batteries. The focus of this study has been on fresh lithium-ion cells, further studies will need to be conducted in order to determine what compensations must be made for cell degradation which will also impact the ToF of the first echo peak.

ORCID

Rhodri E. Owen https://orcid.org/0000-0002-1246-2988
James B. Robinson https://orcid.org/0000-0002-6509-7769
Thomas G. Tranter https://orcid.org/0000-0003-4721-5941
Paul R. Shearing https://orcid.org/0000-0002-1387-9531
Dan J. L. Brett https://orcid.org/0000-0002-8545-3126

References

1. A. Mahmoudzadeh Andwari, A. Pesiridis, S. Rajoo, R. Martinez-Botas, and V. Esfahanian, *Renew. Sustain. Energy Rev.*, **78**, 414 (2017).
2. L. Lu, X. Han, J. Li, J. Hua, and M. Ouyang, *J. Power Sources*, **226**, 272 (2013).
3. M. Danko, J. Adamec, M. Taraba, and P. Drgona, *Transp. Res. Procedia*, **40**, 186 (2019).
4. D. N. T. How, M. A. Hannan, M. S. Hossain Lipu, and P. J. Ker, *IEEE Access*, **7**, 136116 (2019).
5. M. A. Hannan, M. S. H. Lipu, A. Hussain, and A. Mohamed, *Renew. Sustain. Energy Rev.*, **78**, 834 (2017).
6. H. Popp, M. Koller, M. Jahn, and A. Bergmann, *J. Energy Storage*, **32**, 101859 (2020).
7. J. O. Majasan, J. B. Robinson, R. E. Owen, M. Maier, A. N. P. Radhakrishnan, M. Pham, T. G. Tranter, Y. Zhang, P. R. Shearing, and D. J. L. Brett, *J. Phys.: Energy*, **3**, 032011 (2021).
8. B. Sood, C. Hendricks, M. Osterman, and M. Pecht, *Electron. Device Fail. Anal.*, **16**, 4 (2014).
9. A. G. Hsieh, S. Bhadra, B. J. Hertzberg, P. J. Gjeltema, A. Goy, J. W. Fleischer, and D. A. Steingart, *Energy Environ. Sci.*, **8**, 1569 (2015).
10. G. Davies, K. W. Knehr, B. Van Tassell, T. Hodson, S. Biswas, A. G. Hsieh, and D. A. Steingart, *J. Electrochem. Soc.*, **164**, A2746 (2017).
11. P. Ladpli, C. Liu, F. Kopsaftopoulos, and F. K. Chang, *ITEC Asia-Pacific 2018 − 2018 IEEE Transp. Electrif. Conf. Expo, Asia-Pacific E-Mobility A Journey from Now Beyond* p. 1 (2018), 10.1109/itec-ap.2018.8433297.
12. P. Ladpli, F. Kopsaftopoulos, R. Nardari, and F.-K. Chang, *Smart Mater. Nondestruct. Eval. Energy Syst.*, **2017**, 1017108 (2017).
13. P. Ladpli, F. Kopsaftopoulos, and F. K. Chang, "in 11th International workshop on structural health monitoring." *Stanford*, (2017).
14. J. B. Robinson, M. Maier, G. Alster, T. Compton, D. J. L. Brett, and P. R. Shearing, *Phys. Chem. Chem. Phys.*, **21**, 6354 (2019).
15. J. B. Robinson et al., *J. Electrochem. Soc.*, **167**, 120530 (2020).
16. J. B. Robinson, M. Pham, M. D. R. Kok, T. M. M. Heenan, D. J. L. Brett, and P. R. Shearing, *J. Power Sources*, **444**, 227318 (2019).
17. H. Popp, M. Koller, S. Keller, G. Glanz, R. Klambauer, and A. Bergmann, *IEEE Access*, **7**, 170992 (2019).
18. W. Chang, R. Mohr, A. Kim, A. Raj, G. Davies, K. Denner, H. Park, and D. Steingart, *J. Mater. Chem. A*, **8**, 16624 (2020).
19. M. T. M. Pham et al., *J. Power Sources*, **470**, 228039 (2020).
20. J. B. Robinson, M. Pham, M. D. R. Kok, T. M. M. Heenan, D. J. L. Brett, and P. R. Shearing, *J. Power Sources*, **444**, 227318 (2019).
21. C. Bommier, Y. Lu, M. Williams, C. Bommier, W. Chang, Y. Lu, J. Yeung, and G. Davies, *Cell Reports Phys. Sci.*, **1**, 100035 (2020).
22. Q. Kellner, E. Hosseinzadeh, G. Chouchelamane, W. D. Widanage, and J. Marco, "Data batter. cycle life test dev. high-performance electr." *Veh. Appl.* (2017), (http://wrap.warwick.ac.uk/94878).
23. Q. Kellner, E. Hosseinzadeh, G. Chouchelamane, W. D. Widanage, and J. Marco, *J. Energy Storage*, **15**, 228 (2018).
24. Y. Wu, Y. Wang, W. K. C. Yung, and M. Pecht, *Electronics*, **8**, 751 (2019).
25. B. Semburg, *Nucl. Instruments Methods Phys. Res. Sect. A Accel. Spectrometers, Detect. Assoc. Equip.*, **604**, S215 (2009).
26. K. Nowacki and W. Kasprzyk, *Int. J. Thermophys.*, **31**, 103 (2010).
27. P. A. Oliveira, R. M. B. Silva, G. C. Morais, A. V. Alvarenga, and R. P. B. C.- Félix, *J. Phys. Conf. Ser.*, **733**, 012040 (2016).
28. D. P. Finegan et al., *Nat. Commun.*, **6**, 6924 (2015).
29. Y. Troxler, B. Wu, M. Marinescu, V. Yufit, Y. Patel, A. J. Marquis, N. P. Brandon, and G. J. Offer, *J. Power Sources*, **247**, 1018 (2014).
30. T. G. Tranter et al., *J. Electrochem. Soc.*, **167**, 110538 (2020).
31. B. Rieger, S. Schlueter, S. V. Erhard, J. Schmalz, G. Reinhart, and A. Jossen, *J. Energy Storage*, **6**, 213 (2016).
32. K. Y. Oh and B. I. Epureanu, *J. Power Sources*, **303**, 86 (2016).
33. K. W. Knehr, T. Hodson, C. Bommier, G. Davies, A. Kim, and D. A. Steingart, *Joule*, **2**, 1146 (2018).
34. Y. Qi, H. Guo, L. G. Hector, and A. Timmons, *J. Electrochem. Soc.*, **157**, A558 (2010).
35. B. Bitzer and A. Gruhle, *J. Power Sources*, **262**, 297 (2014).
36. F. Grimsmann, F. Brauchle, T. Gerbert, A. Gruhle, M. Knipper, and J. Parisi, *J. Energy Storage*, **12**, 132 (2017).
37. M. P. Mercer, C. Peng, C. Soares, H. E. Hoster, and D. Kramer, *J. Mater. Chem. A*, **9**, 492 (2021).